Separation Science and Technology
Publication details, including instructions for authors and subscription information:
http://www.informaworld.com/smpp/title~content=t713708471

The Adsorption and Desorption Breakthrough Behavior of Carbon Monoxide and Carbon Dioxide on Activated Carbon. Effect of Total Pressure and Pressure-Dependent Mass Transfer Coefficients

Kye Soon Hwang[a]; Won Kook Lee[a]
[a] DEPARTMENT OF CHEMICAL ENGINEERING, KOREA ADVANCED INSTITUTE OF SCIENCE AND TECHNOLOGY, TAEJEON, KOREA

To cite this Article Hwang, Kye Soon and Lee, Won Kook(1994) 'The Adsorption and Desorption Breakthrough Behavior of Carbon Monoxide and Carbon Dioxide on Activated Carbon. Effect of Total Pressure and Pressure-Dependent Mass Transfer Coefficients', Separation Science and Technology, 29: 14, 1857 — 1891
To link to this Article: DOI: 10.1080/01496399408002177
URL: http://dx.doi.org/10.1080/01496399408002177

SEPARATION SCIENCE AND TECHNOLOGY, **29**(14), pp. 1857–1891, 1994

The Adsorption and Desorption Breakthrough Behavior of Carbon Monoxide and Carbon Dioxide on Activated Carbon. Effect of Total Pressure and Pressure-Dependent Mass Transfer Coefficients

KYE SOON HWANG and WON KOOK LEE*
DEPARTMENT OF CHEMICAL ENGINEERING
KOREA ADVANCED INSTITUTE OF SCIENCE AND TECHNOLOGY
373-1, KUSONG DONG, YUSUNG GU, TAEJEON, KOREA

ABSTRACT

The adsorption and desorption breakthrough behaviors of carbon monoxide and carbon dioxide on activated carbon at wide ranges of pressure were studied theoretically and experimentally for single component and multicomponent systems. The effects of total pressure, inlet composition, and flow rate on adsorption and desorption curves were also studied. The experimental adsorption and desorption curves could be predicted fairly well by the linear driving force (LDF) model, and the LDF mass transfer coefficients at various operating conditions were determined by matching the theoretical model and experimental breakthrough curves for the single component system. An LDF mass transfer relationship with pressure-dependent mass transfer coefficients calculated from the single component system provides a reasonably good representation of adsorption and desorption data for multicomponent systems, and the correction factor included in the binary Langmuir isotherm gave the better representation of the experimental data. In the multicomponent systems, the effluent concentration of the light component (carbon monoxide) generally overshoots its inlet concentration during the adsorption step, and the heavy component (carbon dioxide) desorption curves in the desorption steps generally exhibited a plateau region.

INTRODUCTION

Separation of a gas mixture by the adsorption process has been widely applied in industry. Pressure swing adsorption (PSA) and thermal swing

* To whom correspondence should be addressed.

adsorption (TSA) are the two most common adsorptive cyclic processes. In the design and optimization of adsorption processes, basic adsorption and desorption breakthrough data are required. An abundance of single component adsorption breakthrough data exist in the literature, and good success has been achieved in modeling of these data.

Garg and Ruthven (1) suggested the general isothermal solution for micropore diffusion control in a molecular sieve adsorption column, and they studied the performance of molecular sieve adsorption columns when adsorption rates were controlled by micropore diffusion (2) and by macropore diffusion (3).

In contrast to the extensive interest in adsorption breakthrough curves, little attention has been paid to the desorption steps despite its commercial importance. The important aspect of desorption breakthrough curves has been discussed for the single sorbate case by Zwiebel et al. (4). They suggested general numerical solutions for adsorption and desorption curves when the system is isothermal, dilute, controlled by fluid film mass transfer resistance, and has Langmuir-type isotherms. Basmadjian et al. (5) studied nonisothermal desorption by gas purge of single solutes based on equilibrium theory, and Schork and Fair (6) studied thermal regeneration of adsorption beds.

Because of the physical complexity and the mathematical difficulty, little work with multicomponent adsorption has been reported. Ruthven (7), and more recently Yang (8), provided excellent reviews of multicomponent adsorption, particularly that based on equilibrium theory.

Basmadjian et al. (9–11) studied isothermal fixed-bed sorption based on equilibrium theory and different type of isotherms. But adsorption and desorption curves predicted by equilibrium theory give only an approximate representation of the behavior found in real systems.

Cooney and Lightfoot (12) proved the existence of a constant pattern behavior for multicomponent sorption, and Cooney and Strusi (13) obtained analytical solutions for the concentration profiles of two solutes with a constant pattern behavior. Miura and Hashimoto (14) investigated analytical solutions for the breakthrough curves of bicomponent fixed-bed adsorption under the Langmuir isotherm, and Miura et al. (15) suggested a method for calculating breakthrough curves of bicomponent fixed-bed adsorption under a constant pattern and a linear driving force.

Collins and Chao (16) demonstrated the feasibility of calculating both the adsorption and desorption behavior from a dynamic model for nonequilibrium, adiabatic, multicomponent systems. They calculated the mass and heat transfer rates by lumping the resistance of a gas film and intraparticle diffusion. Unfortunately, no experimental data were provided for comparing the calculation results.

Zwiebel et al. (17) presented the first generalized depletion data for multicomponent systems with nonlinear isotherms. A mathematical model was also presented with assumptions of a fluid film mass transfer mechanism and Langmuir-type isotherms, but few experimental data were provided for comparing the calculation results.

Recently, Huang and Fair (18, 19) reported the adsorption of ethane–propane mixtures from nitrogen or helium, and the regeneration of the mixtures using a purge of hot nitrogen or helium. They also developed a mathematical model for nonequilibrium, nonisothermal, and nonadiabatic systems with a linear driving force (LDF) mass transfer relationship and variable lumped-resistance coefficients. They gave good guidelines for predicting thermal swing cycles.

Although a number of models for predicting the adsorption and desorption curves have been proposed by many investigators, relatively little experimental data have been reported. Furthermore, since the adsorption separation processes involve the adsorption of multicomponent mixtures, multicomponent data are required.

The objectives of this work are to obtain the experimental adsorption and desorption breakthrough curves of carbon monoxide, carbon dioxide, and their mixtures on activated carbon at various pressure ranges, to investigate the effect of operating variables for adsorption and desorption processes, and to provide information for adsorptive separation processes, such as PSA.

The goals of this research include the validity of the well-known LDF approximation and Langmuir equilibrium isotherm in numerical simulation of fixed-bed dynamics by comparing experimental adsorption and desoption curves for multicomponent systems as well as single component systems.

MATHEMATICAL MODEL

The LDF Model

The linear driving force (LDF) model is an approximation to the solution of Fick's diffusion equation for a spherical particle. This expression assumes that the mass transfer rate of adsorption is proportional to the difference between the equilibrium concentration and the actual concentration of the component. Since the solution of the LDF rate model is much easier and faster than the solution of a diffusion model, this approximation has found widespread applications (6, 15, 18, 22, 24, 28).

When the mass transfer rate is controlled by intraparticle diffusion, then the mass transfer coefficient, k, must be considered as a lumped parameter. This has been discussed by Gluekauf (25) who showed that,

for linear systems, $k \approx 15D_e/r_p^2$. Equivalent relationships for nonlinear systems have been developed by Ruthven et al. (29).

LDF rate expressions have been used to represent the mass transfer resistance in the mathematical model because of computational simplicity. In order to develop a mathematical model to analyze the experimental results and fixed-bed dynamics, the following approximations are introduced.

1. The ideal gas law applies.
2. The pressure gradient across the bed is neglected.
3. The system is isothermal.
4. The interstitial velocity is constant during the adsorption and desorption steps.
5. The flow pattern is described by the axial dispersed plug flow model.
6. The mass transfer rate is represented by a linear driving force rate expression.
7. The equilibrium relationship for the adsorbing component is represented by the Langmuir isotherm.

Applying the above assumptions to the component balance of the gas phase through a packed bed, the following equation is obtained.

$$-D_{Li}\frac{\partial^2 C_i}{\partial_z^2} + \nu\frac{\partial C_i}{\partial_z} + \frac{\partial C_i}{\partial t} + \frac{1-\epsilon}{\epsilon}\rho_p\frac{\partial q_i}{\partial t} = 0 \tag{1}$$

The mass transfer rate of gas and solid phase can be expressed as the following linear driving force model.

$$\partial q_i/\partial t = k_i(q_i^* - q_i) \tag{2}$$

In this case the mass transfer coefficients are lumped parameters and such a linearized expression is generally accepted as fairly accurate (6, 15, 18, 22, 24, 28). The equilibrium isotherm can be represented by the following Langmuir-type equation.

$$\frac{q_i^*}{q_{si}} = \frac{(b_i/\eta_i)Py_i}{1 + \sum_{j=1}^{2} b_jPy_j/\eta_j} \tag{3}$$

In the above equation, q_{si} is the saturation value of q_i^* for component i, and b_i is the equilibrium constant. The η_i is a correction factor for the binary Langmuir isotherm. The binary Langmuir equations can be improved by introducing η_i, which actually indicates interspecies interactions. Boundary conditions at $Z = 0$ and $Z = L$ and for $t > 0$ are

$$D_{Li}\frac{\partial C_i}{\partial Z}\bigg|_{Z=0} = -\nu\left(C_i\Big|_{Z=0^-} - C_i\Big|_{Z=0^+}\right) \tag{4}$$

$$\left.\frac{\partial C_i}{\partial Z}\right|_{Z=L} = 0 \tag{5}$$

The associated initial conditions are as follows for $0 < Z < L$:

$$C_i(Z, 0) = 0;\ q_i(Z, 0) = 0 \qquad \text{(adsorption)} \tag{6}$$

$$C_i(Z, 0) = C_{i,\text{in}};\ q_i(z, 0) = q_{i,\text{in}} \qquad \text{(desorption)} \tag{7}$$

The initial gas and solid phase concentrations for the adsorption step are zero. For the desorption step, they are the values of the final conditions of the previous adsorption step. Applying the ideal gas law and introducing appropriate dimensionless variables, Eqs. (1)–(7) are written as follows:

$$\frac{\partial Y_i}{\partial \tau} = \frac{1}{\text{Pe}_i}\frac{\partial^2 Y_i}{\partial X^2} - \frac{\partial Y_i}{\partial X} - \Phi_i \frac{\partial Q_i}{\partial \tau} \tag{8}$$

$$\frac{\partial Q_i}{\partial \tau} = \alpha_i(Q_i^* - Q_i) \tag{9}$$

$$Q_i^* = \frac{\beta_i \gamma_i Y_i}{1 + \sum_{j=1}^{2} \gamma_i Y_i} \tag{10}$$

Boundary conditions

$$\left.\frac{\partial Y_i}{\partial X_i}\right|_{X=0} = -\text{Pe}_i\left(\left.Y_i\right|_{X=0^-} - \left.Y_i\right|_{X=0^+}\right) \tag{11}$$

$$\left.\frac{\partial Y_i}{\partial X_i}\right|_{X=1} = 0 \tag{12}$$

Initial conditions

$$Y_i(X, 0) = 0;\ Q_i(X, 0) = 0 \qquad \text{(adsorption)} \tag{13}$$

$$Y_i(X, 0) = 1;\ Q_i(X, 0) = 1 \qquad \text{(desorption)} \tag{14}$$

In the above equations the dimensionless parameters are defined as follows.

$$Y_i = y_i/y_{i,\text{in}}, \quad Q_i = q_i/q_{i,\text{in}}, \quad Q_i^* = q_i^*/q_{i,\text{in}}, \quad X = Z/L, \quad \tau = \nu t/L,$$

$$\text{Pe}_i = \nu L/D_{\text{L}i}, \quad \Phi_i = RTq_{i,\text{in}}\rho_p(1 - \epsilon)/P/y_{i,\text{in}}/\epsilon, \quad \alpha_i = k_i L/\nu,$$

$$\beta_i = q_{si}/q_{i,\text{in}}, \quad \gamma_i = Pb_i y_{i,\text{in}}/\eta_i$$

The simultaneous solution of Eqs. (8)–(12) with initial conditions gives the adsorption and desorption breakthrough curves.

Parameter Estimation

The partial differential equations (PDEs) representing the fixed-bed system dynamics were solved by the method of orthogonal collocation. The partial differential equations were first reduced to a set of ordinary differential equations (ODEs) by the method of orthogonal collocation (20, 21).

The resulting set of ODEs were then solved numerically in the time domain by using DGEAR of the International Mathematics and Statistical Library (IMSL). This program employs Gear's stiff method with variable order and step size. Seven collocation points were used in this work. The details of the collocation form of these equations are discussed elsewhere (22).

In order to simulate the fixed-bed dynamics and match the experimental response curves, numerical values for the dimensionless groups listed in the previous section are required. Bed length, bed voidage, fluid velocity, system temperature, total pressure, and feed concentration are directly measurable operation variables. The Langmuir parameters for carbon monoxide and carbon dioxide on activated carbon were determined experimentally from the pure component adsorption isotherms.

The other two parameters are the axial dispersion coefficient and the LDF mass transfer coefficient. The axial dispersion coefficients for the different experimental runs were estimated from the correlation given by Hsu and Haynes (23):

$$\frac{1}{\mathrm{Pe}} = \frac{0.328}{\mathrm{ReSc}} + \frac{3.33}{1 + 0.59(\mathrm{ReSc})^{-1}} \tag{15}$$

Only one parameter, the LDF mass transfer coefficient, remains to be determined by matching the theoretical model and the experimental breakthrough curves. The LDF mass transfer coefficient was determined directly by matching the pure component experimental adsorption and desorption curves. A trial-and-error procedure was used.

In the numerical simulation of a multicomponent system, an LDF mass transfer relationship with pressure-dependent mass transfer coefficients calculated from the single component system was used, and in the binary Langmuir isotherm a correction factor was introduced to predict adsorption and desorption data for the multicomponent system more accurately.

EXPERIMENTAL SYSTEM

Fixed-Bed Experiment

The system selected in the present study was adsorption of carbon monoxide and carbon dioxide on activated carbon. Norit B4 activated

carbon was used as an adsorbent. Its physical properties are presented in Table 1 together with details of the bed characteristics. Helium was used as the carrier gas in the adsorption step and as the purge gas during the desorption step. Both adsorbates, carbon monoxide and carbon dioxide, were more than 99.9% pure, and the helium was of chromatographic grade (99.999%). The feed gas was a premixed gas, and the composition of the premixed gas was verified by gas chromatography.

A schematic diagram of the fixed-bed experimental setup is presented in Fig. 1. The adsorption vessel was fabricated from stainless steel and was 60 cm long with a 50 cm packed section, 3.7 cm (inside) diameter. The remaining sections at both ends of the adsoption column were 5 cm long and filled with glass wool to ensure uniform gas distribution and to prevent the carryover of adsorbent particles.

To maintain an uniform bed temperature, a water jacket was installed around the adsorption vessel and two K-type thermocouples were installed above and below the column to check the inlet and outlet gas temperatures. All the experiments were carried out at 298 K, and the temperature of the system was monitored. No significant temperature deviations were observed.

The gas flow to the column was controlled by a mass flow controller (Unit Instrument Co., Model UFC-1100A) with a readout power supply (Model URS 100-5) which was precalibrated against a soap bubble flowmeter covering a wide range of flow rates under experimental pressures.

The system was controlled and maintained at constant pressure with a backpressure regulator (Tescom, Model 44-4763-24). The system total pressure was monitored with two pressure transducers (Cole-Parmer Instrument Co., Model SA) installed above and below the column, and the results were displayed on a digit readout (Model 7350-34).

TABLE 1
Physical Properties of Adsorbent and Bed Characteristics

BET surface area (m^2/g)	1100–1200
Pore size distribution:	
Micropores (<1 nm)	0.42
Transition pores (1–100 nm)	0.09
Macropores (>100 nm)	0.49
Particle density (g/cm^3)	0.82
Particle size (cm)	0.1–0.15
Bed length (cm)	60
Bed diameter (cm)	3.7
Bed bulk density (g/cm^3)	0.47
Bed void fraction	0.41

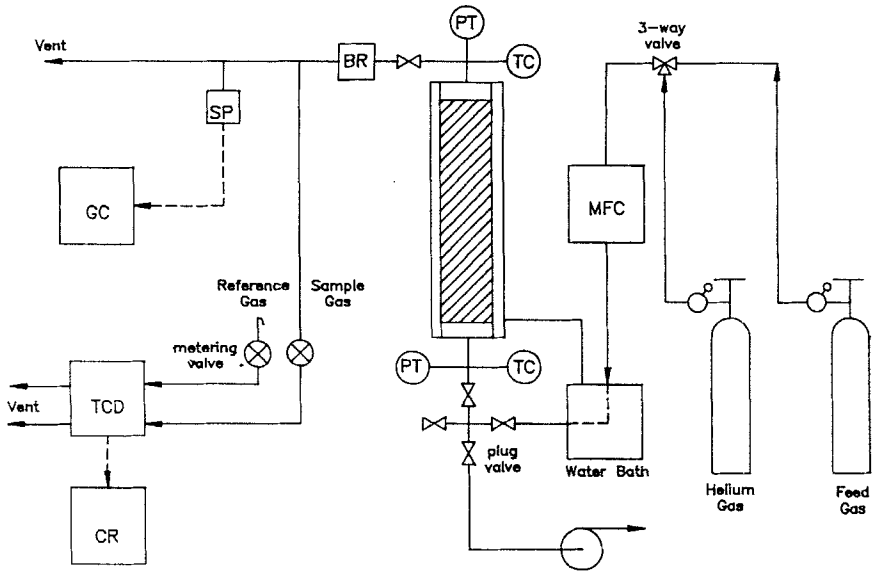

BR : Back pressure regulator, GC : Gas Chromatograph, MFC : Mass flow controller, PT : Pressure transducer, CR : Chart recorder, SP : Sampling port, TC : Thermocouple, TCD : Thermal conductivity detector

FIG. 1 A schematic diagram of the fixed-bed experimental setup.

The sorbate concentration in the exit stream for single component systems was monitored continuously by a thermister-type thermal conductivity detector (Gow-Mac, Model 10-677) which had been calibrated with mixtures of known compositions. In the multicomponent system, the thermister-type thermal conductivity cell was used for easy reading of concentration history, and simultaneously an HP 5890A gas chromatography (GC) with the thermal conductivity detector was used to analyze the bed effluents. A Porapack Q packed column was used to analyze helium, carbon monoxide, and carbon dioxide with hydrogen carrier gas. The retention times of the chromatograms under our conditions of interest were less than 2 minutes. Gas samples were taken from a sampling port which was fitted with septa for syringes. The syringes were equipped with locks, and samples could be collected at short intervals and stored for later GC analysis.

Prior to an experiment, the packed column was cleaned by a mechanical vacuum pump under helium purge. The required flow (by mass flow controller) and corresponding system pressure (by backpressure regulator)

were adjusted with helium, and a sufficiently long time was allowed for the thermal conductivity detector (TCD) baseline to stabilize and the column temperature to become uniform. The flow of helium gas was then replaced by the feed gas by switching the 3-way valve.

The effluent concentrations were monitored continuously on the strip chart recorder through the thermal conductivity cell. After completing the adsorption run (after the bed was saturated with the feed concentration), the 3-way valve was switched to the helium purge gas and the desorption run was followed in the same manner as the adsorption run. In this way both adsorption and desorption breakthrough curves were obtained for each run. Details of the experimental procedure for the pure component system can be found elsewhere (24)

In multicomponent experiments the same methods as for the single component system were used, but detailed concentration analyses were required by GC. In order to analyze the effluent concentrations in more detail, we used syringes equipped with locks.

Equilibrium Measurement

The equilibrium adsorption isotherms for carbon monoxide and carbon dioxide on Norit B4 activated carbon were measured in our laboratory with a volumetric-type apparatus. A static equilibrium technique was used for the measurement of the pure gas adsorption isotherms. Pure component equilibrium isotherms of carbon monoxide and carbon dioxide were measured at 298 K, and the results are shown in Fig. 2. The isotherms of carbon monoxide and carbon dioxide are of the favorable type (concave downward), and carbon dioxide is more favorable and strongly adsorbed on activated carbon than is carbon monoxide.

The carbon monoxide and carbon dioxide data could be fitted to Langmuir isotherms. The Langmuir parameters for carbon monoxide and carbon dioxide at 298 K and the correction factors for the binary Langmuir isotherm are given in Table 2.

RESULT AND DISCUSSION

Single Component System

Sixteen adsorption and desorption runs were made with pure carbon monoxide and carbon dioxide. Details of the operating conditions for the pure component system are listed in Table 3. The run numbers of the adsorption and desorption steps are the same numbers; all runs were cyclic and consisted of sequential steps of adsorption and desorption.

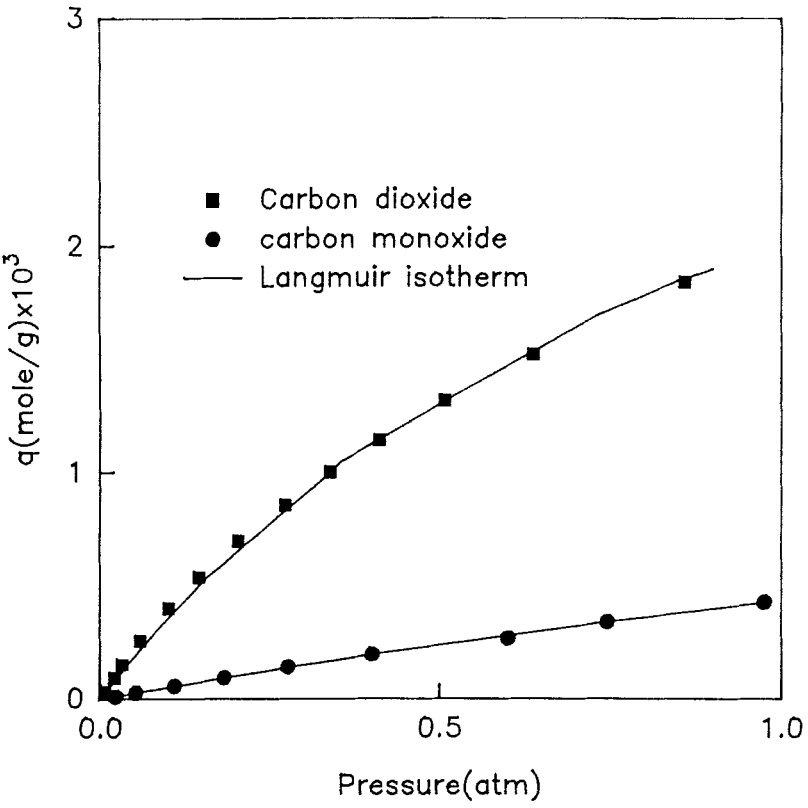

FIG. 2 Adsorption isotherms for carbon monoxide and carbon dioxide on activated carbon at 298 K.

TABLE 2
Langmuir Parameters for Adsorption Isotherms and Binary Langmuir Isotherm Correction Factors

	Carbon monoxide	Carbon dioxide
b (1/atm)	0.34	1.90
$q_s \times 10^3$ (mol/g)	1.99	3.0
η_i	1.18	1.26

TABLE 3
Fixed-Bed Operating Conditions for Single Component System.

	Adsorption step				Desorption step				
Run	Adsorbate	y_{in}	P (atm)	F^a (cm^3/min)	Inert	P (atm)	F^a (cm^3/min)	Purge	$k \times 10^2$ (s^{-1})
AD1	CO_2	0.05	15	7500	He	15	7500	He	2.2
AD2	CO_2	0.05	10	5000	He	10	5000	He	3.2
AD3	CO_2	0.05	5	2500	He	5	2500	He	5.2
AD4	CO_2	0.05	10	7500	He	10	7500	He	3.3
AD5	CO_2	0.015	15	7500	He	15	7500	He	1.8
AD6	CO_2	0.015	10	5000	He	10	5000	He	3.0
AD7	CO_2	0.015	5	2500	He	5	2500	He	6.1
AD8	CO_2	0.015	3	1500	He	3	1500	He	11.0
AD9	CO_2	0.015	1	500	He	1	500	He	18.5
AD10	CO	0.04	3	1500	He	3	1500	He	70.0
AD11	CO	0.04	15	7500	He	15	7500	He	20.2
AD12	CO	0.04	10	5000	He	10	5000	He	27.3
AD13	CO	0.04	5	2500	He	5	2500	He	42.7
AD14	CO	0.04	10	3500	He	10	3500	He	26.5
AD15	CO	0.04	5	5000	He	5	5000	He	32.0
AD16	CO	0.02	10	5000	He	10	5000	He	27.0

[a] At 1 atm, 298 K.

A typical adsorption–desorption cycle for carbon dioxide at 10 atm total pressure is illustrated in Fig. 3. The y_{out}/y_{in} represents the mole fraction ratio of feed to outlet for the adsorbate. The fit of the LDF mass transfer model to the experimental curves is also presented in Fig. 3. We selected the mass transfer coefficients values which were good fits for both the adsorption and desorption curves. The calculated values of the LDF mass transfer coefficient for each run are contained in Table 3.

As can be seen in Fig. 3, the LDF model provides a reasonably good representation of both adsorption and desorption curves. This figure also shows that the depletion point appears before the adsorption breakthrough point, and the desorption curves are significantly broader (more tailing) than the adsorption breakthrough curves. The same results were obtained for carbon monoxide, but the asymmetry is more significant for carbon dioxide than for carbon monoxide.

Garg and Ruthven (1–3) reported that the relative rates of adsorption and desorption are greatly affected by the nonlinearity of the equilibrium isotherm. From equilibrium data, the carbon monoxide and carbon dioxide isotherms are favorable, and therefore unfavorable for desorption. The adsorption and desorption curves for carbon monoxide and carbon dioxide

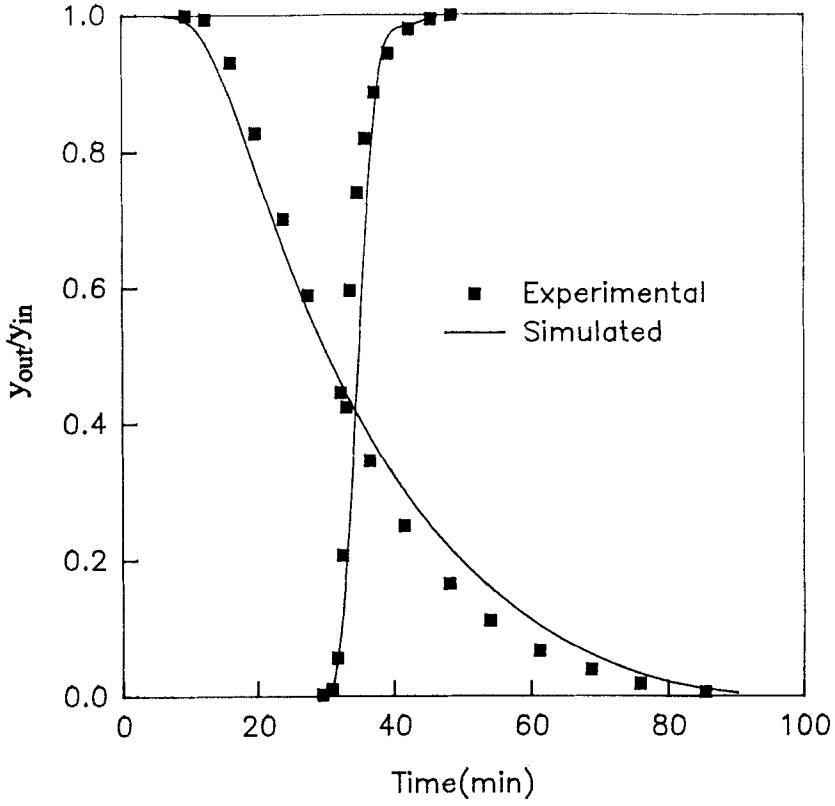

FIG. 3 Typical adsorption and desorption curves for carbon dioxide (Run AD2).

showed asymmetry, and this asymmetry is more significant for carbon dioxide than for carbon monoxide because the carbon dioxide isotherm is more favorable.

Figure 4 represents the adsorption and desorption mass transfer rate for Run AD2 at $X = 0.5$ and the mass transfer rates calculated from the single component rate equation plotted as a function of time. The magnitude of the desorption rate is initially higher, and therefore the depletion point appears sooner than the breakthrough point. As time proceeds, the adsorption rates reach considerably higher values than do the desorption rates, which causes sharper breakthrough profiles. The peak values of the desorption rate is reached earlier than that of adsorption, thus the maximum slope of the depletion curve precedes the steepest portion of the corresponding breakthrough curve. The desorption rate recedes more slowly than the adsorption rate, resulting in an extended tail of the deple-

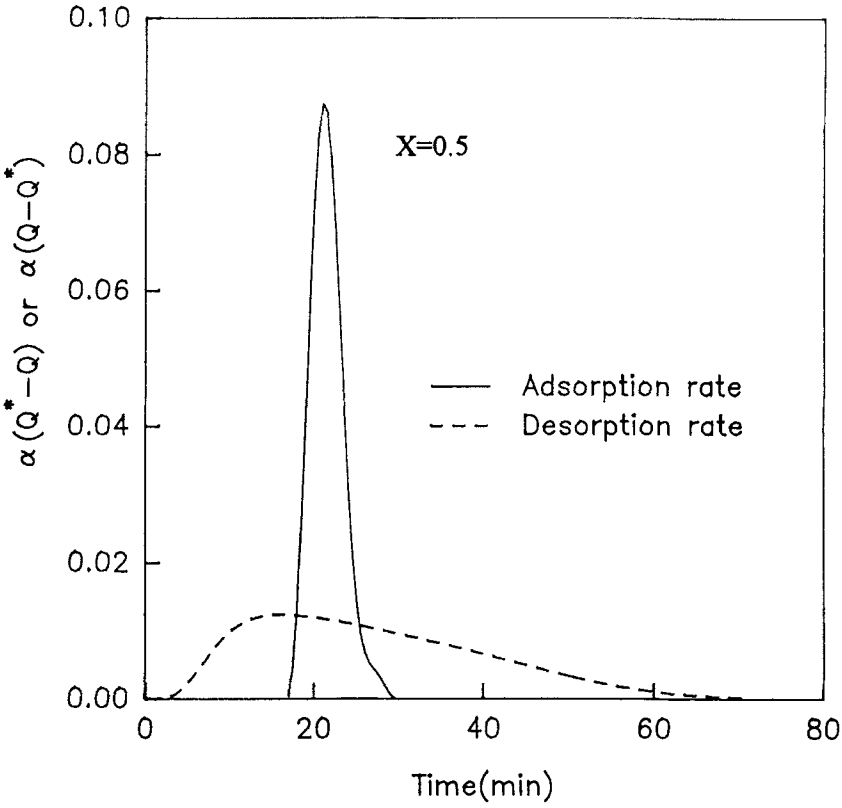

FIG. 4 Adsorption and desorption mass transfer rates (based on simulation for Run AD2).

tion profiles. These agree with the observations reported by Zwiebel et al. (4).

The effect of total bed pressure at constant flow rate is presented in Fig. 5. From Fig. 5 it is observed that the adsorption breakthrough and desorption depletion point appeared later at high pressure. It is clear that the bed-loading capacity increases when the partial pressure of the adsorbate increases. Thus, at constant flow rate the breakthrough time and depletion time increase with increasing pressure.

To analyze the pressure effect, the contact time was maintained constant as the total pressure was varied, which requires varying flow rates. This is illustrated in Fig. 6. In contrast to the constant flow rate, the breakthrough time and depletion times at constant contact time decreased when the total pressure increased. The same results were obtained for carbon monoxide.

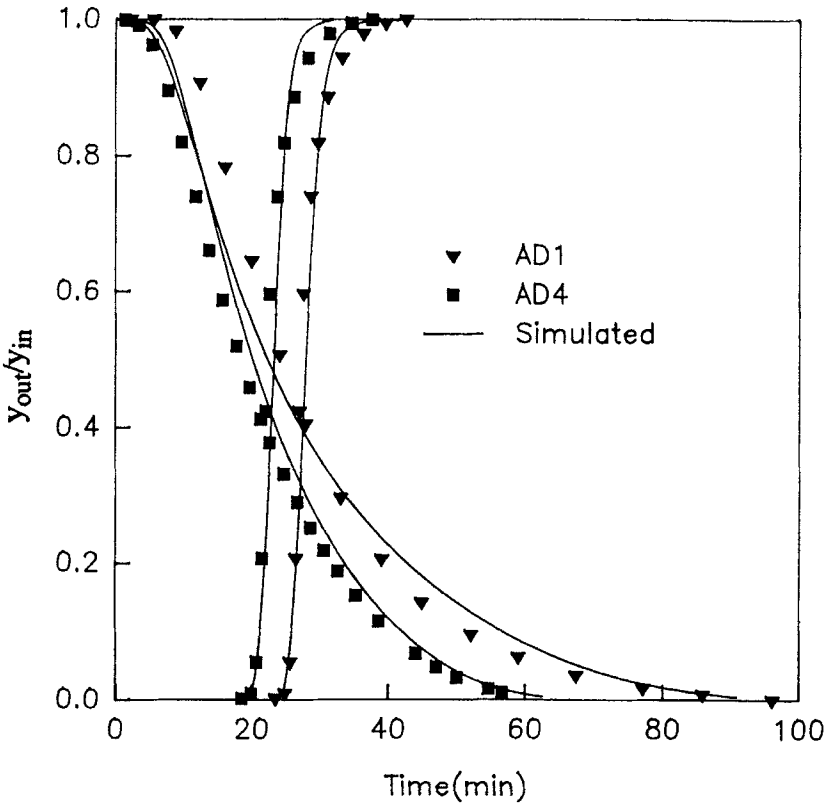

FIG. 5 Effect of pressure on carbon dioxide adsorption and desorption curves at constant flow rate (Run AD1, P = 15 atm; Run AD4, P = 10 atm).

The mass flow rates must increase linearly with increasing pressure to maintain the same contact time at different pressures, but the bed-loading capacity does not increases linearly with pressure. In these systems, the bed-loading capacity varies along with the Langmuir isotherm equation. Therefore, the breakthrough point and depletion point appeared earlier when the total pressure increased at constant contact time.

It is also observed from Fig. 6 that the breakthrough and depletion curves were broadened as pressure increased, and this was more pronounced in the desorption processes. This means that the mass transfer rates of carbon dioxide decreased with increasing pressure. Thus the LDF mass transfer coefficients calculated from the experimental curves are smaller when the system pressure is high.

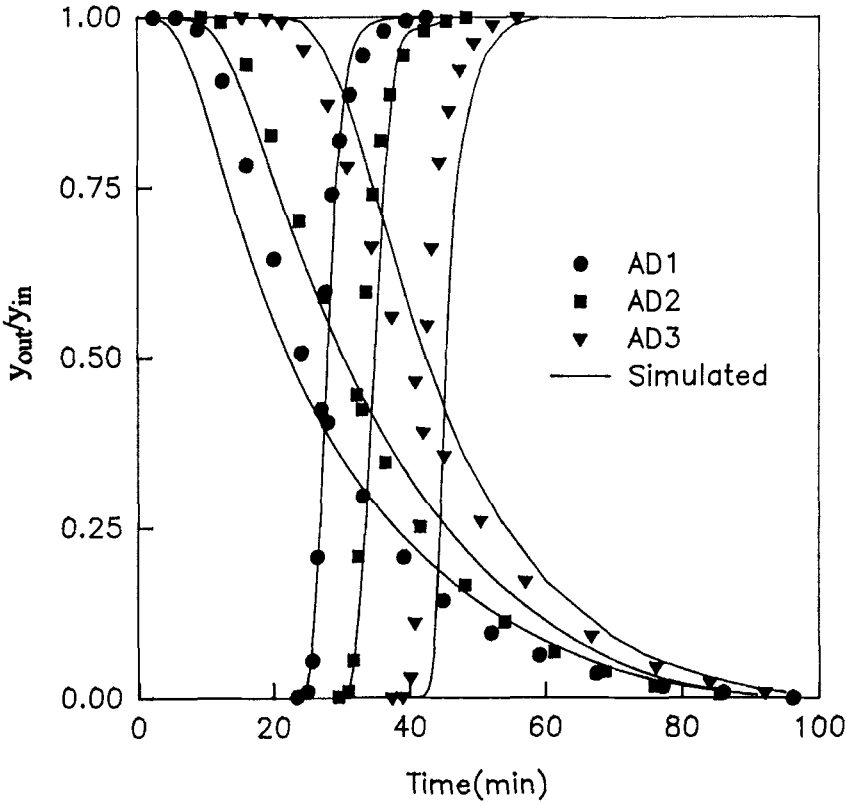

FIG. 6 Effect of pressure on carbon dioxide adsorption and desorption curves at constant contact time (Run AD1, P = 15 atm; Run AD2, P = 10 atm; Run AD3, P = 5 atm).

The effects of feed concentration on adsorption and desorption curves are illustrated in Fig. 7 for carbon monoxide, and the effects of flow rates on carbon dioxide adsorption and desorption curves are presented in Fig. 8.

The variation of inlet composition and flow rate result in shorter breakthrough and depletion times with increasing inlet compositions and flow rate. The rate at which a sorbate travels along the column depends on the product of the fluid velocity and the sorbate concentration in the fluid phase. For a favorable isotherm the ratio of the fluid phase to the adsorbed phase concentrations increases with the concentrations, so that the sorbate moves more rapidly when the concentration and flow rate are high.

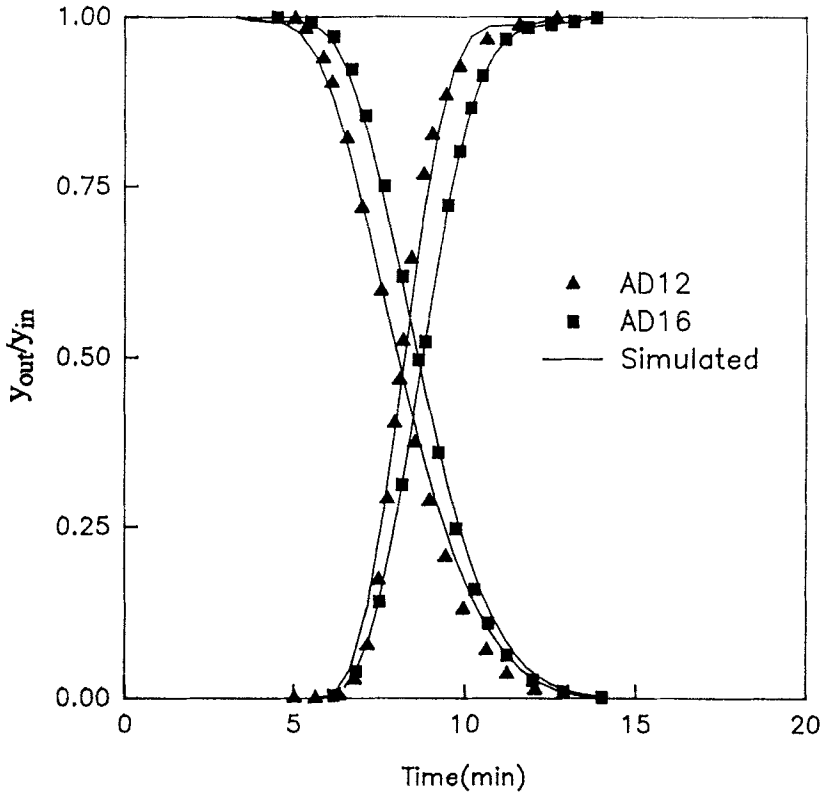

FIG. 7 Effect of feed composition on carbon monoxide adsorption and desorption curves (Run AD12, $y_{in} = 0.04$; Run AD16, $y_{in} = 0.02$).

The LDF Mass Transfer Coefficient

Since the classical work of Glueckauf (25), the LDF expression has been examined by a number of investigators from different points of view, and it has been widely used in the analysis of chromatography and packed-bed adsorbers.

Liaw et al. (26) and Rice (27) showed that the LDF expression can be derived by assuming a parabolic profile for the adsorbate concentration within the pellet in an approximate solution of the intraparticle diffusion equation. The main advantages of the LDF approximation are in its greatly simplified use for unsteady-state diffusion in porous particles and in its reduced computation complexity.

As mentioned earlier, the LDF mass transfer coefficients in the present

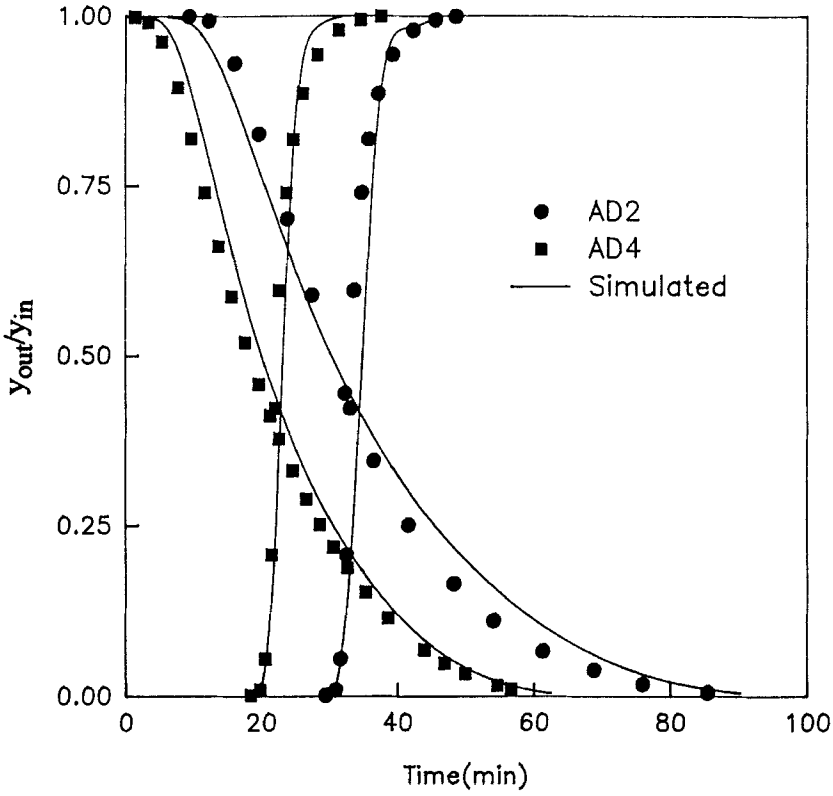

FIG. 8 Effect of flow rate on carbon dioxide adsorption and desorption curves (Run AD2, F = 5000 cm^3/min; Run AD4, F = 7500 cm^3/min).

work were determined directly by matching the theoretical model and the experimental adsorption and desorption curves. We have selected the values of mass transfer coefficients which fitted both the adsorption and desorption curves.

For a porous adsorbent, there are three resistances which may contribute to the overall mass transfer resistance: the external fluid film resistance, the macropore diffusional resistance, and the micropore diffusional resistance. Depending on the particular system and conditions, any one of the three potential resistances to mass transfer may be controlling. Indeed, more than one resistance may be important (7). If the controlling resistance is macropore diffusion in the molecular regime, the mass transfer coefficient is inversely proportional to pressure, while within the

Knudsen diffusion regime or conditions of micropore control, the mass transfer coefficient will be effectively independent of pressure (22).

As illustrated in experimental data, for this system the mass transfer coefficients are strongly affected on the total pressure compared with the feed concentration or flow rate. These results indicate that the dominant mass transfer resistance in this system is macropore diffusion in the molecular regime.

Figures 9 and 10 show the pressure dependence of the mass transfer coefficient calculated from experimental curves for carbon dioxide and carbon monoxide, respectively. The overall mass transfer coefficients decrease with increasing pressure, and under comparable conditions the overall mass transfer coefficients for carbon dioxide are much smaller than those for carbon monoxide.

We obtained the following correlation equations for carbon monoxide

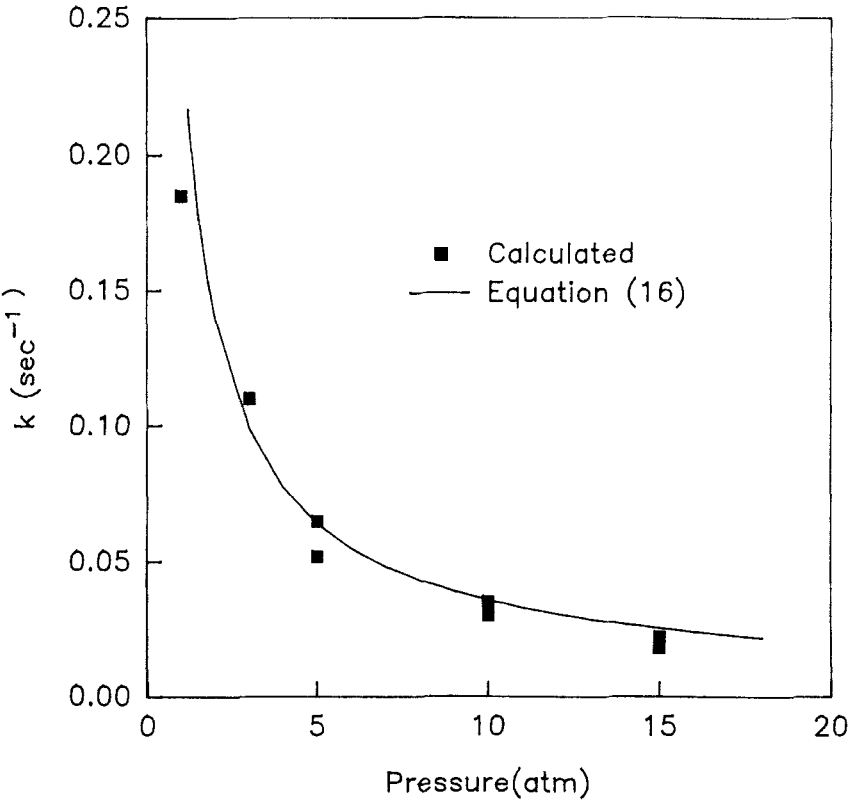

FIG. 9 Pressure-dependent LDF mass transfer coefficient for carbon dioxide.

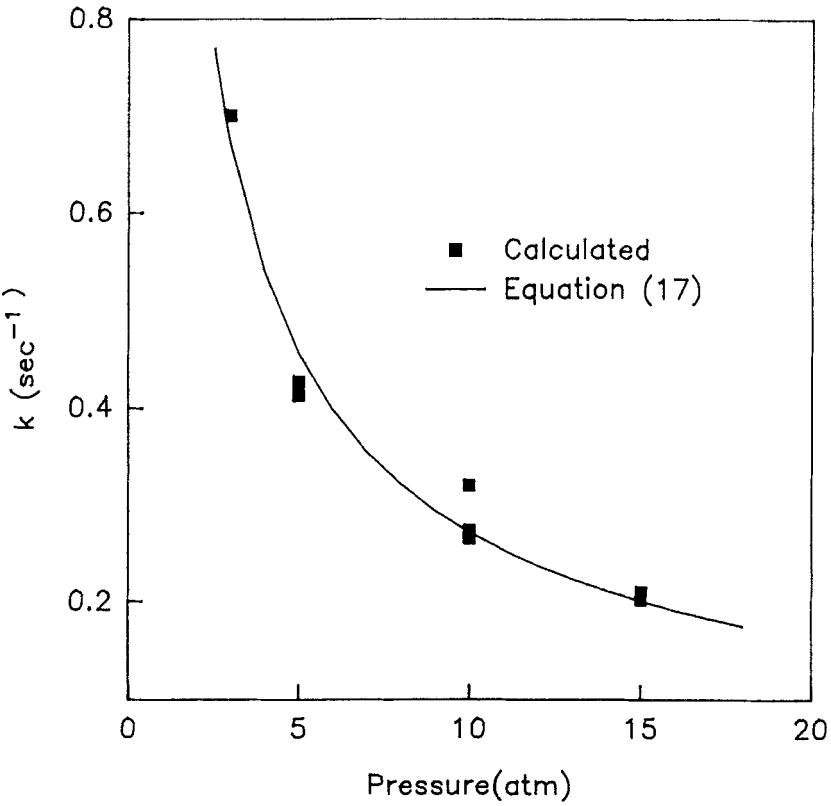

FIG. 10 Pressure-dependent LDF mass transfer coefficient for carbon monoxide.

and carbon dioxide from best curve fitting. For carbon dioxide:

$$k = 0.25/P^{0.85} \tag{16}$$

For carbon monoxide:

$$k = 1.53/P^{0.75} \tag{17}$$

In the numerical simulation of multicomponent systems, an LDF mass transfer relationship with pressure-dependent mass transfer coefficients calculated from a single component system was used

Multicomponent System

In experiments for multicomponent systems, 12 adsorption and desorption runs were performed. The operating conditions are summarized in

Table 4. The run numbers for adsorption and desorption steps correspond with each other; all runs were cyclic and consisted of sequential steps of adsorption and desorption.

In the numerical simulation of multicomponent system, an LDF mass transfer relationship with pressure-dependent mass transfer coefficients calculated from a single component system was used, and in the binary Langmuir isotherm we introduced a correction factor to predict the adsorption and desorption data for multicomponent systems fairly well.

A typical adsorption cycle run for a multicomponent system (Run BA3) is presented in Fig. 11. The $y_{i,out}/y_{i,in}$ represent the mole fraction ratio of feed to outlet for each adsorbate, and the dashed and solid curves represent the calculated results from the binary Langmuir and corrected binary Langmuir isotherms, respectively. As can be seen in Fig. 11, the adsorption breakthrough curve of the heavy component (carbon dioxide) is sig-

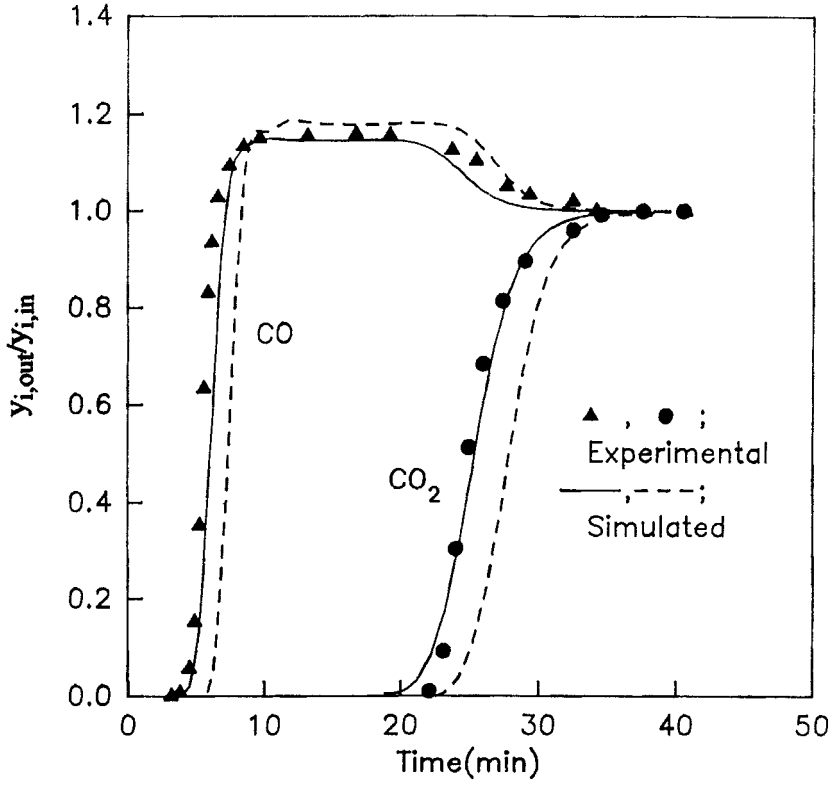

FIG. 11 Typical adsorption breakthrough curve for multicomponent system. (- -) Langmuir isotherm; (——) corrected Langmuir isotherm, based on Run BA3.

moidal, as was the case in the single component system. However, the breakthrough curve of the light component (carbon monoxide) is entirely different from that of the pure component adsorption process. The effluent concentration of carbon monoxide rises very rapidly after it break through, and it overshoots its inlet composition.

Figure 11 also shows that the experimental curves of adsorption and desorption for multicomponent systems could be predicted fairly well by the LDF model, and the corrected binary Langmuir isotherm gave better representation of the experimental data than did the binary Langmuir isotherm.

As shown in Fig. 11, the binary Langmuir isotherm overpredicted the carbon monoxide roll-up value, and the breakthrough times of carbon monoxide and carbon dioxide were predicted to be much later than the experimental data actually showed. It has been shown that the binary Langmuir isotherm is thermodynamically unsound. Despite its lack of a rigorous thermodynamic basis and the inbuilt weakness of the Langmuir model itself, the binary Langmuir equation is widely used for modeling adsorber dynamics, largely because of its mathematical simplicity.

We therefore introduced a correction factor, η_i, which actually indicates the interspecies interactions to predict the adsorption and desorption data for multicomponent systems fairly well. Hereafter, all the simulations for multicomponent systems are presented by the corrected binary Langmuir isotherm. From Fig. 11 it is also clear that an LDF mass transfer relationship with pressure-dependent mass transfer coefficients calculated from a single component system provides a reasonably good representation of adsorption and desorption data for a multicomponent system.

To obtain a fundamental understanding of roll-up behavior, the bed profile at different times for Run BA3 is shown in Fig. 12. This figure shows the dimensionless gas-phase concentration of the light component (carbon monoxide) and the heavy component (carbon dioxide) as a function of dimensionless bed length. The light component moves more quickly than the heavy component, and it is displaced or purged from the adsorbent while the heavy component is adsorbed in its place.

For short period of time after the feed is admitted, roll-up of the light component is not fully developed while the heavy component concentration profile is developing. As time goes on, the roll-up of carbon monoxide is develops and the adsorbed carbon monoxide is displaced by the newly arriving carbon dioxide molecules. As further time elapses, carbon dioxide starts to break through, and the roll-up value of carbon monoxide becomes less evident. When carbon dioxide completely breaks through, the concentration of carbon monoxide decreases to its inlet composition, and thereafter both adsorbates travel through the bed with feed compositions.

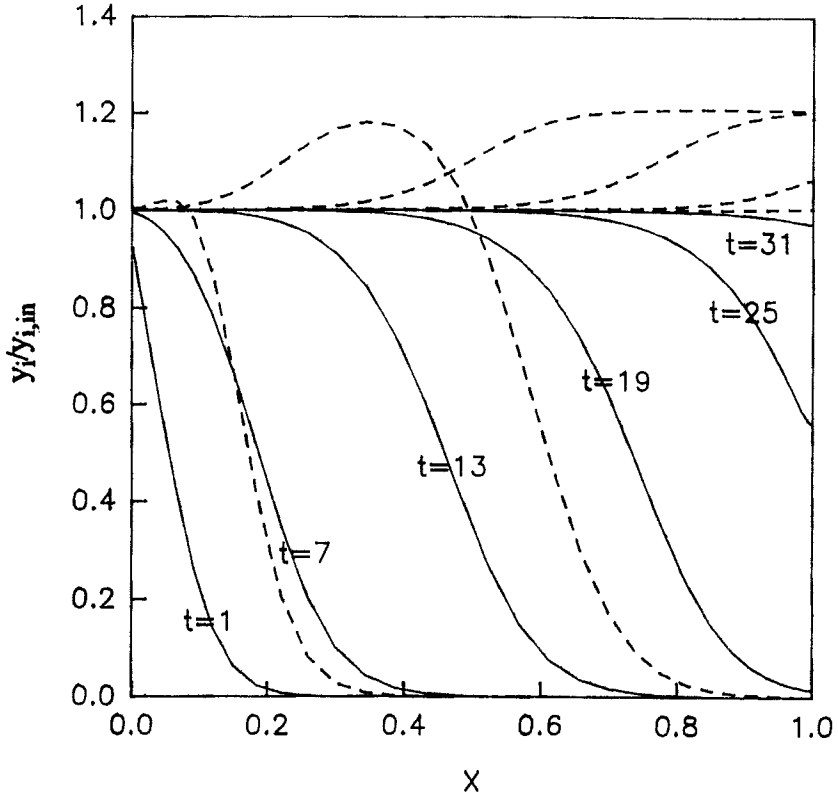

FIG. 12 Propagation of concentration front in adsorption step for multicomponent system. (- -) Carbon monoxide; (——) carbon dioxide, based on simulation for Run BA3.

thereafter both adsorbates travel through the bed with feed compositions.

After the bed was saturated with adsorbates in the previous adsorption step, the desorption process was started by using a helium purge. A typical desorption cycle run for a multicomponent system (Run BD3) is presented in Fig. 13. The ordinate of Fig. 13 is the ratio of effluent concentrations of the desorption run to inlet concentrations of the corresponding previous adsorption run. Hereafter, all figures of desorption curves are presented in this same scale.

In contrast with adsorption where the light component curves display overshoots above the feed concentration, in desorption processes the heavy component desorption curves exhibit a dip of plateau region. The desorption curves of the light component (carbon monoxide) are similar to the desorption curves of a single component system. Zwiebel et al. (17)

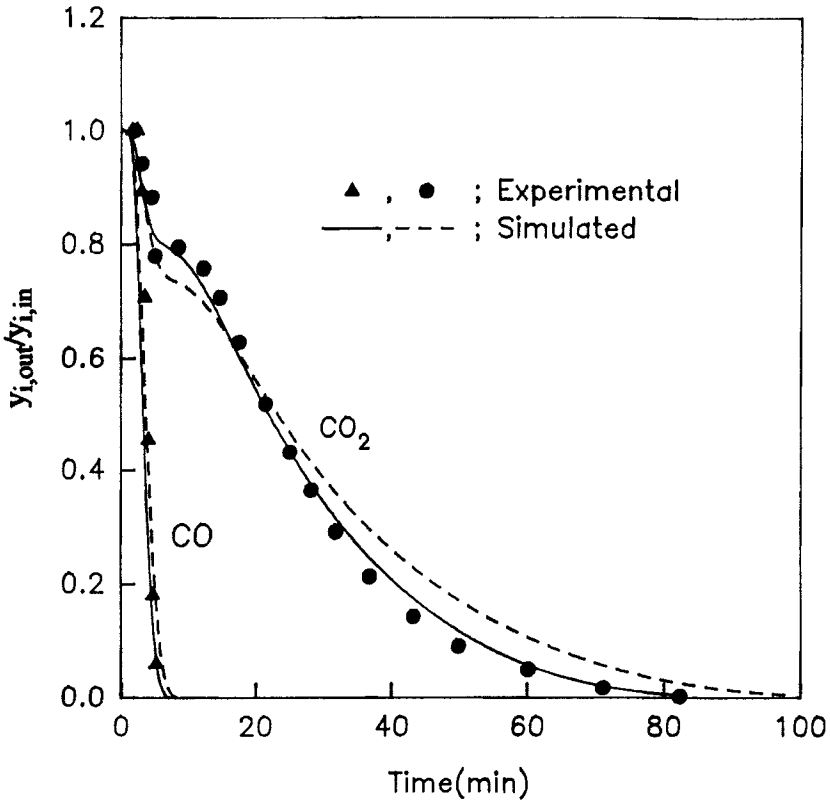

FIG. 13 Typical desorption breakthrough curve for multicomponent system. (- -) Langmuir isotherm; (——) corrected Langmuir isotherm, based on Run BD3.

reported this plateau region as "instabilities," and Huang and Fair (18) referred to the "dip" in the thermal regeneration process.

After complete breakthrough of carbon dioxide in the previous adsorption step, only a fraction of the carbon monoxide is left in the bed. Thus, the desorption curves of carbon monoxide drop rapidly. Conversely, since most of the bed is saturated with carbon dioxide, the desorption time for carbon dioxide is much longer. These influences can be seen more clearly in Fig. 14 which gives the dimensionless gas-phase concentration of the light component (carbon monoxide) and the heavy component (carbon dioxide) for the desorption process as a function of dimensionless bed length. A few minute after the desorption step starts, the carbon monoxide is completely desorbed. On the other hand, the carbon dioxide concentration history in the bed is different from that of carbon monoxide. In the

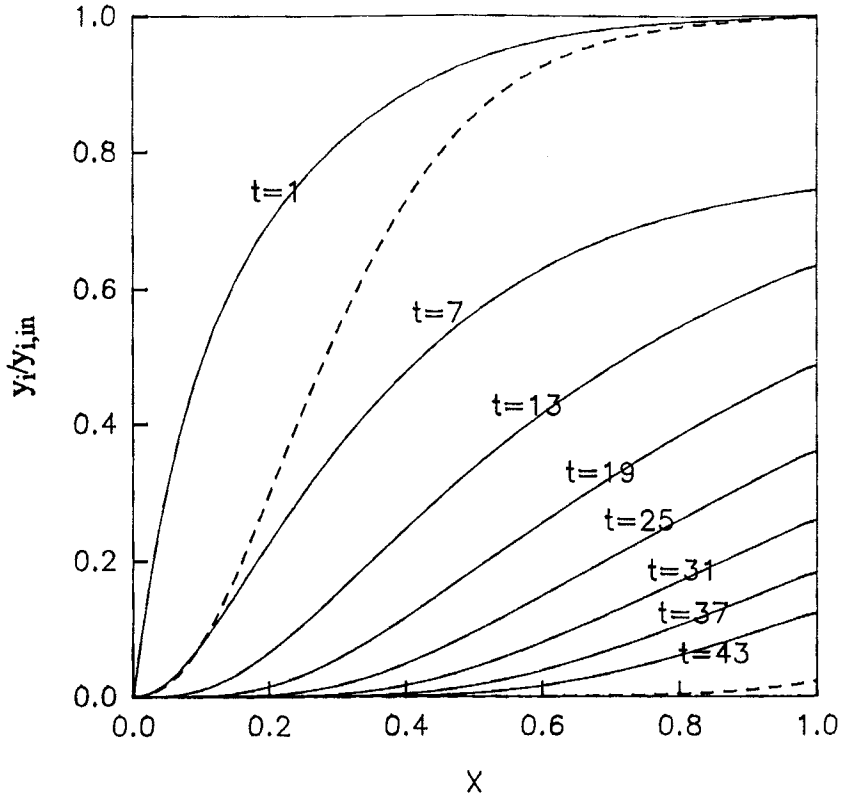

FIG. 14 Propagation of concentration front in desorption step for multicomponent system. (- -) Carbon monoxide; (——) carbon dioxide, based on simulation for Run BD3.

lowered rapidly, but after a few minutes its concentration lowers very slowly.

As mentioned above, since only a fraction of the carbon monoxide is left in the bed after complete breakthrough of carbon dioxide in the previous adsorption step, and since carbon monoxide is a weakly adsorbed sorbate, the desorption rate of carbon monoxide drop rapidly as the sorbate is depleted. As the purge gas initially enters the saturated bed, it removes adsorbates from the bed void volume. The carbon dioxide in the bed void volume is removed very quickly, the effluent concentration of carbon dioxide drops to a certain value, and then the carbon dioxide molecules purged upstream are readsorbed on downstream sites. This cause a plateau in the carbon dioxide desorption curves.

The effect of total pressure in a bed at a constant flow rate on the adsorption breakthrough curves is presented in Fig. 15. The breakthrough times of both adsorbates increase with pressure at a constant flow rate as in the single component system, and this is more significant for carbon dioxide. Since carbon dioxide is the more strongly adsorbed component, the pressure effect on its breakthrough is more significant. However, the height of roll-up is increased with pressure. As the total pressure increases, the amount of heavy component (carbon dioxide) adsorbed increases. Accordingly, the carbon monoxide molecules are more easily displaced by carbon dioxide molecules when the system pressure increases.

The effect of bed pressure at a constant contact time (a constant interstitial velocity) is illustrated in Fig. 16. As shown in Table 4, Runs BA1 and

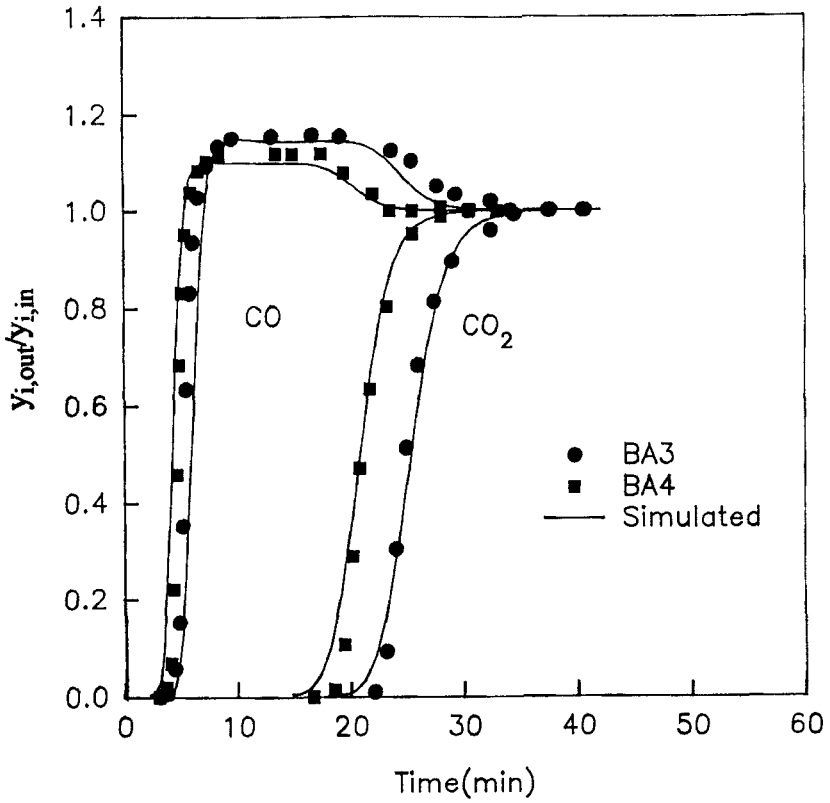

FIG. 15 Effect of pressure on adsorption curves for multicomponent system at constant flow rate (Run BA3, P = 15 atm; Run BA4, P = 10 atm).

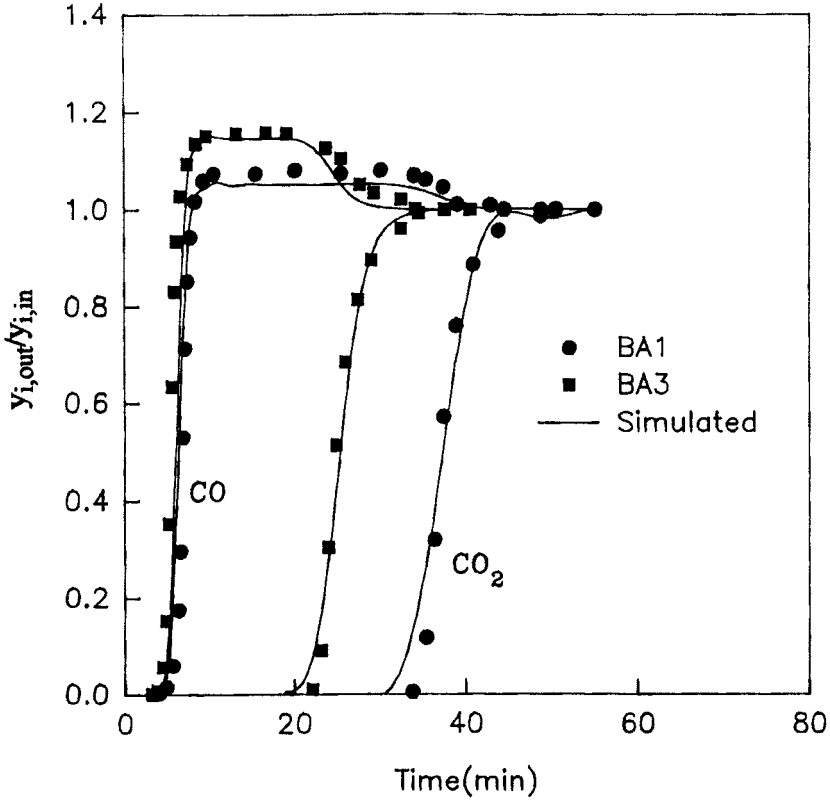

FIG. 16 Effect of pressure on adsorption curves for multicomponent system at constant contact time (Run BA1, P = 5 atm; Run BA3, P = 15 atm).

TABLE 4
Fixed-Bed Operating Conditions for Multicomponent System

Adsorption step						Desorption step			
Run	$y_{CO,in}$	$y_{CO_2,in}$	P (atm)	F^a (cm^3/min)	Inert	Run	P (atm)	F^a (cm^3/min)	Purge
BA1	0.05	0.05	5	2500	He	BD1	5	2500	He
BA2	0.05	0.05	10	5000	He	BD2	10	5000	He
BA3	0.05	0.05	15	7500	He	BD3	15	7500	He
BA4	0.05	0.05	10	7500	He	BD4	10	7500	He
BA5	0.03	0.05	10	5000	He	BD5	10	5000	He
BA6	0.05	0.027	10	5000	He	BD6	10	5000	He

[a] At 1 atm, 298 K.

BA3 were operated under the same interstitial velocity, but the system pressure for Run BA1 was 5 atm and for Run BA3 was 15 atm. As seen in Fig. 16, the carbon monoxide roll-up is higher for Run BA3 than for Run BA1. Thus, we can conclude from Figs. 15 and 16 that for the separation of carbon monoxide and carbon dioxide, a higher system pressure is favorable.

The effect of pressure on the desorption curves at a constant contact time is presented in Fig. 17 for Runs BD1 and BD3. Figure 17 shows that the value of the dip or plateau region is lowered when the pressure in the system is increased. This is because relatively large amount of adsorbates exist in the bed void volume in the previous adsorption step when the system pressure is high. In the next desorption step, a relatively large amount of the carbon dioxide in the bed void volume is removed in the

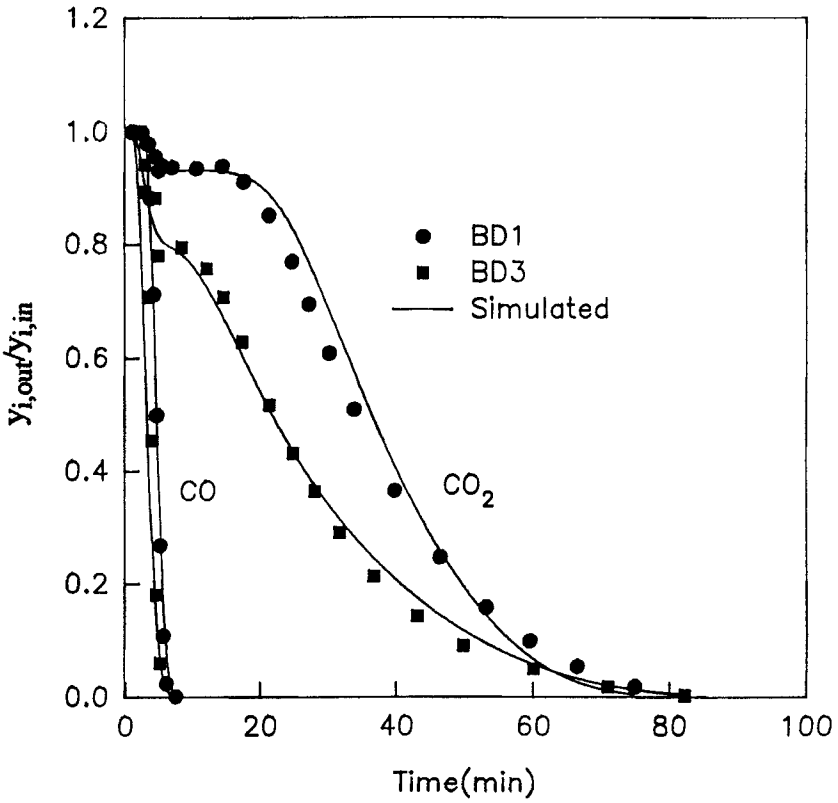

FIG. 17 Effect of pressure on desorption curves for multicomponent system at constant contact time (Run BD1, P = 5 atm; Run BD3, P = 15 atm).

initial time period when the system pressure is high. This results in a low plateau value at high pressure.

Figures 18 and 19 illustrate the effect of the inlet concentrations of carbon dioxide and carbon monoxide, respectively. As Fig. 18 shows, the higher the carbon dioxide inlet concentrations, the higher the carbon monoxide roll-ups and the earlier the carbon dioxide and carbon monoxide breakthroughs. The height of roll-up increases with increasing carbon dioxide concentration at a constant carbon monoxide feed level. The heavy component has a greater competitive capability at a higher concentration. Consequently, more of the light component is displaced downstream.

On the other hand, as shown in Fig. 19, the overshoot decreases with increasing carbon monoxide concentration at a constant carbon dioxide

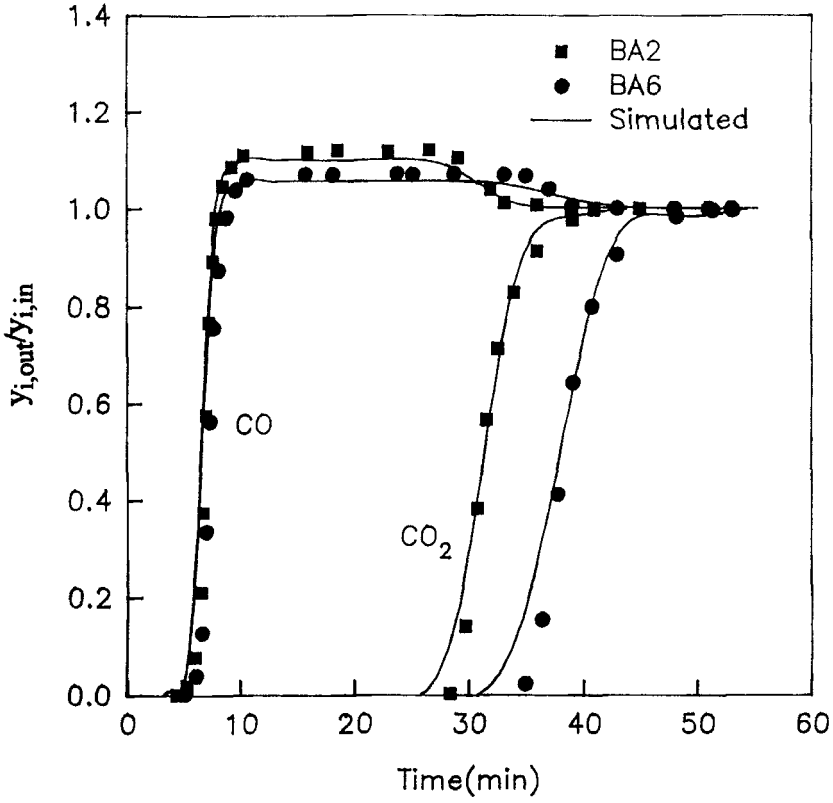

FIG. 18 Effect of carbon dioxide inlet composition on adsorption curves for multicomponent system (Run BA2, $y_{CO_2,in} = 0.05$; Run BA6, $y_{CO_2,in} = 0.027$).

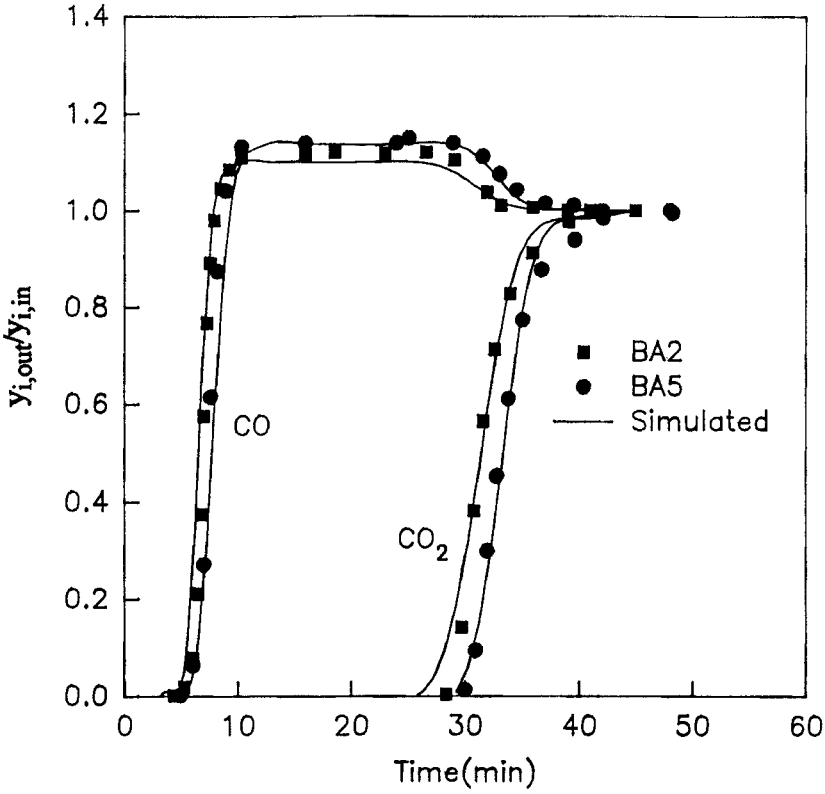

FIG. 19 Effect of carbon monoxide feed composition on adsorption curves for multicomponent system (Run BA2, $y_{CO,in} = 0.05$; Run BA5, $y_{CO,in} = 0.03$).

feed level. This is the result of the relative competition between adsorbates. The light component adsorbabilities decrease with increasing concentration since the light component is more readily displaced by the heavy component at a downstream location.

It is clear from Figs. 18 and 19 that the higher the inlet concentrations of carbon monoxide and carbon dioxide, the earlier breakthrough occurs. The effect of inlet concentration is more significant for carbon dioxide than for carbon monoxide. For a system with a favorable isotherm, the loading capacity of adsorbent increases along with the gas-phase concentration, although the increase is not linear. The loading capacity increment due to the increasing inlet concentration of carbon dioxide was significant compared to its total loading capacity. For carbon monoxide, however, the loading capacity increment was trivial compared to its total loading capacity.

The shape of the breakthrough curve of the heavy component remains the same for both single-component and multicomponent adsorption process, and is little affected by the light component. The effect of varying the light component concentration on the complete breakthrough time of the key component is small. Varying the heavy component feed concentration has a much more significant effect on its breakthrough curves. Gariepy and Zwiebel (28) and Huang and Fair (19) reported similar findings with regard to the inlet composition effect.

The effect of flow rate on adsorption and desorption breakthrough curves is illustrated in Figs. 20 and 21, respectively. As shown in Fig. 20, a change of flow rate has little effect on the roll-up of carbon monoxide, but the higher the flow rate, the earlier adsorbate breakthrough occurs. Since a larger flow rate bring more adsorbates into the bed per unit time,

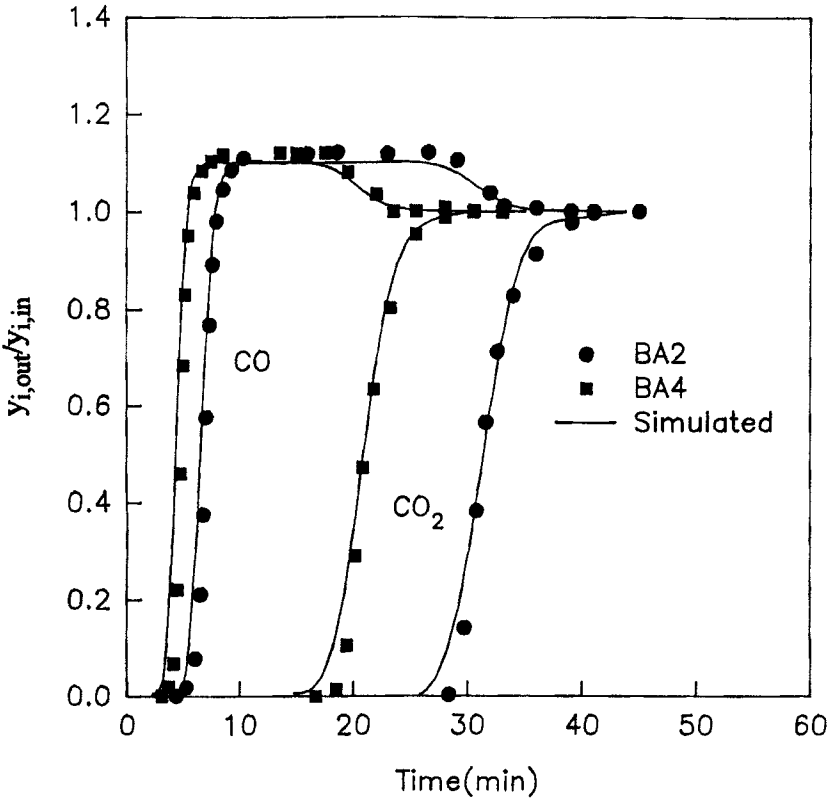

FIG. 20 Effect of flow rate on adsorption curves for multicomponent system (Run BA2, F = 5000 cm^3/min; Run BA4, F = 7500 cm^3/min).

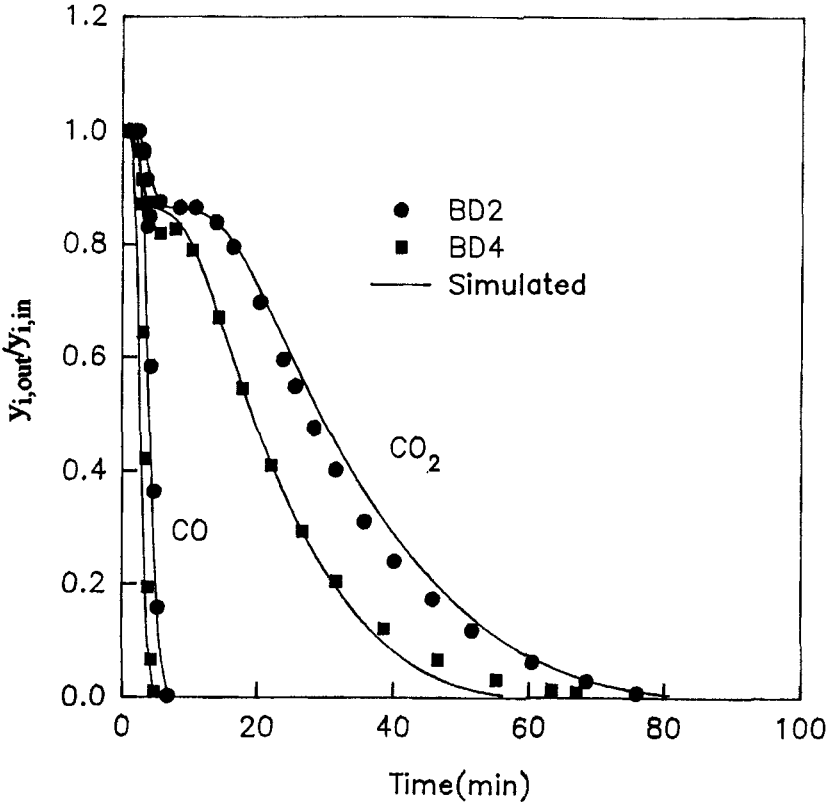

FIG. 21 Effect of flow rate on desorption curves for multicomponent system (Run BD2, F = 5000 cm^3/min; Run BD4, F = 7500 cm^3/min).

breakthrough is expected to be earlier. The time difference between carbon dioxide and carbon monoxide breakthrough increases for a low flow rate. From Fig. 21 it is also clear that increasing the purge rate shifts the peak position of the carbon dioxide desorption curve to the left, and that decreases the regeneration time. Generally, in adsorptive separation processes, an increase of the purge rate results in a shorter regeneration time but the use of more purge gas. Therefore, the optimal purge rate must be determined for a given system.

CONCLUSIONS

The adsorption and desorption breakthrough curves for carbon monoxide and carbon dioxide on activated carbon were determined experimen-

tally at wide ranges of pressure for single and multicomponent systems. The LDF mass transfer coefficients at various operating conditions were determined by matching the theoretical model and experimental breakthrough curves for the single component system.

The experimental adsorption and desorption curves could be predicted fairly well by the LDF model, and in the multicomponent system the correction factor included in the binary Langmuir isotherm gave a better representation of the experimental data. Based on an analysis of the experimental and modeling results, the following conclusions are drawn.

The desorption points generally appear before the corresponding breakthrough points, and the desorption profiles are significantly broader than the corresponding adsorption curves. The breakthrough time and depletion time increase with pressure at a constant flow rate but decrease with pressure at a constant contact time. Both the adsorption and desorption of the carbon monoxide/carbon dioxide/activated carbon system are found to be macropore-mass-transfer-controlled processes. The overall mass transfer coefficients for carbon dioxide are much smaller than for carbon monoxide. A linear driving force mass transfer relationship with pressure-dependent mass transfer coefficients calculated from the single component system provides a reasonably good representation of adsorption and desorption data for multicomponent systems.

In multicomponent systems the effluent concentration of the light component (carbon monoxide) generally overshoots its inlet concentration during the adsorption step because of the displacement by the heavy component (carbon dioxide). The height of roll-up increases with the total pressure of the system and the inlet composition of the heavy component, but decreases with the inlet composition of the light component.

In contrast with adsorption where the light component curves display overshoots above the feed concentration, heavy component desorption curves in desorption processes exhibit a plateau region. The values of the plateau region decrease with increasing system pressures and flow rates.

For the separation of carbon monoxide and carbon dioxide by the adsorption process, a higher total pressure is favorable. A high system pressure, however, is unfavorable for desorption.

SYMBOLS

b_i Langmuir isotherm constant for component i (1/atm)

C_i adsorbate concentration of component i in the gas phase (g·mol/cm^3)

$C_{i,\text{in}}$ adsorbate concentration of component i in the feed (g·mol/cm^3)

d_p particle diameter (cm)

D_e effective diffusion coefficient (cm^2/s)
D_L axial dispersion coefficient for component i (cm^2/s)
D_m molecular diffusivity (cm^2/s)
F flow rate at 1 atm and 298 K (cm^3/min)
k_i LDF mass transfer coefficient for component i (1/s)
L bed length (cm)
P total pressure (atm)
Pe_i $= \nu L/D_L$, Peclet number for component i
Pe' $= \nu d_p/D_L$, particle Peclet number
q_i adsorbate concentration of component i in the solid phase (g·mol/g)
$q_{i,in}$ value of q at equilibrium with $y_{i,in}$ (g·mol/g)
q_i^* value of q at equilibrium with y_i (g·mol/g)
q_{si} saturation concentration of component i (g·mol/g)
Q_i $= q_i/q_{i,in}$, dimensionless adsorbate concentration of component i in the solid phase
r_p particle radius (cm)
R gas constant
Re $= d_p \epsilon \nu \rho_g/\mu$, Reynolds number
Sc $= \mu/(\rho_g D_m)$, Schmidt number
t time
T temperature, K
ν interstitial velocity (cm/s)
X $= z/L$, dimensionless axial distance
y_i mole fraction of component i in the gas phase
$y_{i,in}$ mole fraction of component i in the feed gas
y_{out} mole fraction of pure component at $X = 1$
$y_{i,out}$ mole fraction of component i at $X = 1$
Y_i $= y_i/y_{i,in}$, dimensionless mole fraction of component i in the gas phase
Z axial distance coordinate (cm)

Greek Letters

α_i $= k_i L/\nu$, dimensionless parameter for component i
β_i $= q_{si}/q_{i,in}$, dimensionless parameter for component i
ϵ bed void fraction
γ_i $= P y_{i,in} b_i/\eta_i$, dimensionless parameter for component i
Φ_i $= (1 - \epsilon) RT \rho_p q_{i,in}/P/y_{i,in}/\epsilon$, dimensionless parameter for component i
η_i correction factor for component i in binary Langmuir isotherm
μ viscosity

ρ_g density of gas (g/cm^3)
ρ_p particle density (g/cm^3)
τ $= \nu t/L$, dimensionless parameter

Superscript

* equilibrium

Subscripts

i component *i*
in feed
out outlet
p particle

REFERENCES

1. D. R. Garg and D. M. Ruthven, *Chem. Eng. Sci.*, *28*, 799 (1973).
2. D. R. Garg and D. M. Ruthven, *Ibid.*, *29*, 571 (1974).
3. D. R. Garg and D. M. Ruthven, *Ibid.*, *29*, 1961 (1974).
4. I. Zwiebel, C. M. Kralik, and J. J. Schnitzer, *AIChE J.*, *18*, 1139 (1972).
5. D. Basmadjian, K. D. Ha, and C. Y. Pan, *Ind. Eng. Chem., Process Des. Dev.*, *14*, 328 (1975).
6. J. M. Schork and J. R. Fair, *Ind. Eng. Chem. Res.*, *27*, 457 (1988).
7. D. M. Ruthven, *Principles of Adsorption and Adsorption Processes*, Wiley, New York, 1984.
8. R. T. Yang, *Gas Separation by Adsorption Processes*, Butterworths, Boston, 1987.
9. D. Basmadjian and P. Coroyannakis, *Chem. Eng. Sci.*, *42*, 1723 (1987).
10. D. Basmadjian, P. Coroyannakis, and C. Karayannopoulos, *Ibid.*, *42*, 1737 (1987).
11. D. Basmadjian, C. Karayannopoulos, and P. Coroyannakis, *Ibid.*, *42*, 1753 (1987).
12. D. O. Cooney and E. N. Lightfoot, *Ind. Eng. Chem., Fundam.*, *4*, 233 (1965).
13. D. O. Cooney and F. P. Strusi, *Ibid.*, *11*, 123 (1972).
14. K. Miura and K. Hashimoto, *J. Chem. Eng. Jpn.*, *12*, 329 (1979).
15. K. Miura, H. Kurahashi, Y. Inokuchi, and K. Hashimoto, *Ibid.*, *12*, 281 (1979).
16. H. W. Collins and K. C. Chao, *AIChE Symp. Ser.*, *69*, 9 (1973).
17. I. Zwiebel, C. M. Kralik, and J. J. Schnitzer, *AIChE J.*, *20*, 915 (1974).
18. C. C. Huang and J. R. Fair, *Ibid.*, *34*, 1861 (1988).
19. C. C. Huang and J. R. Fair, *Ibid.*, *35*, 1667 (1989).
20. J. Villadsen and M. L. Michelsen, *Solution of Differential Equation Models by Polynomial Approximation*, Prentice-Hall, Englewood Cliffs, New Jersey, 1978.
21. B. A. Finlayson, *Nonlinear Analysis in Chemical Engineering*, McGraw-Hill, New York, 1980.
22. N. S. Raghavan, M. M. Hassan, and D. M. Ruthven, *AIChE J.*, *31*, 385 (1985).
23. L. K. P. Hsu and H. W. Haynes, *Ibid.*, *27*, 81 (1981).
24. S. Farooq and D. M. Ruthven, *Ind. Eng. Chem. Res.*, *29*, 1084 (1990).
25. E. Glueckauf, *Trans. Faraday Soc.*, *51*, 1540 (1955).
26. C. H. Liaw, J. S. P. Wang, R. A. Greenkorn, and K. C. Chao, *AIChE J.*, *25*, 376 (1979).

27. R. G. Rice, *Chem. Eng. Sci.*, *37*, 83 (1982).
28. R. L. Gariepy and I. Zwiebel, *AIChE Symp. Ser.*, *67*, 17 (1971).
29. D. M. Ruthven and D. R. Garg, *AIChE J.*, *21*, 200 (1975).

Received by editor June 1, 1993
Revised November 12, 1993